

Ultrafast switching of photonic entanglement

Matthew A. Hall,¹ Joseph B. Altepeter,¹ and Prem Kumar¹

¹*Center for Photonic Communication and Computing, EECS Department
Northwestern University, 2145 Sheridan Road, Evanston, IL 60208-3118*

Harnessing the existing telecommunications infrastructure to distribute entangled photons would provide a dramatic reduction in the overhead needed to deploy and operate a quantum network. The traditionally empty 1310-nm telecommunications band is uniquely suited for this task. However, an additional resource is required to realize such a network: a switch capable of routing single photons at high speeds, with minimal loss and signal-band noise, and—most importantly—without disturbing the photons’ quantum state. These exacting requirements preclude the use of all previous switching technologies. Here we present a switch which fulfills these requirements and characterize its performance at the single photon level; it exhibits a 200-ps switching window, a 120:1 contrast ratio, < 1 dB loss, and induces no measurable degradation in the switched photons’ entangled-state fidelity (< 0.002). In addition, we demonstrate its utility by successfully demultiplexing a single quantum channel from a dual-channel, time-division-multiplexed entangled photon stream.

PACS numbers:

Switching technologies enable networked rather than point-to-point communications. Next-generation photonic quantum networks will require switches that operate with low loss, low signal-band noise, and *without* disturbing the transmitted photons’ spatial, temporal, or polarization degrees of freedom [1]. Additionally, the switch’s operational wavelength must be compatible with a low-loss, non-dispersive transmission medium, such as the standard optical fiber’s 1.3- μ m zero-dispersion band [2, 3]. Unfortunately, no previously demonstrated technology [4]–[15] is capable of *simultaneously* satisfying each of the above requirements: waveguide electro-optic modulators (EOMs) [16] and resonators [17, 18] can operate at very high speeds (10 GHz) but completely destroy any quantum information stored in the polarization degree of freedom; micro-electromechanical switches [6, 19] do not degrade the photon’s quantum state, but operate at very low speeds (\leq 250 kHz); polarization-independent EOMs [16] can operate at moderate speeds (\sim 100 MHz) but with relatively high loss; and finally, traditional 1550-nm devices based on nonlinear-optical fiber loops [7, 20] generate unacceptably high levels of Raman-induced noise photons ($>$ 1 in-band noise photon per 100-ps switching window [21]).

Although the requirements for ultrafast entangled-photon switching are collectively daunting, they describe a device that is capable of selectively coupling the spatial and temporal degrees of photonic quantum information. In other words, a device that can encode multiple-qubit quantum states onto a single photon, enabling quantum communication protocols that exploit high-dimensional spatio-temporal encodings. In this Letter we describe the construction and characterization of an all-optical switch which meets each of the aforementioned requirements, and whose aggregate performance (in terms of loss, speed, and in-band noise) exceeds that of all available alternatives [4]–[20] by orders of magnitude [22].

Moreover, we utilize this switch to demonstrate demultiplexing of a single quantum channel from a dual-channel, time-division-multiplexed entangled photon stream.

In order to achieve simultaneously low-loss and ultrafast switching, we utilize an all-optical, fiber-based design in which bright 1550-nm pump (C-band) pulses control the trajectory of 1310-nm (O-band) single-photon signals (see Figure 1(b)). Physically, this switch exploits polarization-insensitive cross-phase modulation (XPM) [23] in a nonlinear-optical loop mirror (NOLM) [24], the reflectivity of which is determined by the phase difference between the clockwise and counter-clockwise propagating paths in a fiber Sagnac interferometer (the “loop”) [25]. In order to actively control the state of this switch, we initially configure an intra-loop fiber polarization controller such that the loop *reflects* all incoming photons. Multiplexing a strong 1550-nm pump pulse into the clockwise or counter-clockwise loop path then creates an XPM-induced phase shift on the respective clockwise or counter-clockwise signal amplitude, with a π phase shift causing the switch to *transmit all* incoming photons. As XPM is inherently polarization dependent, and polarization is often used to encode quantum information, it is important that the pump pulse itself be effectively unpolarized. We accomplish this by temporally overlapping two distinct but orthogonally polarized pump wavelengths when creating the control pulses [23].

Note that the traditional NOLM-based C-band devices are unsuitable for single-photon switching for two reasons: Firstly, and most importantly, such switches generate very high levels of Raman-induced background photons at signal wavelengths [21]. These noise photons would swamp any single-photon signals, effectively “washing out” any two-photon quantum correlations. Secondly, traditional NOLM-based devices utilize pump pulses which are group-velocity matched to the signals being switched. While this increases the interaction time,

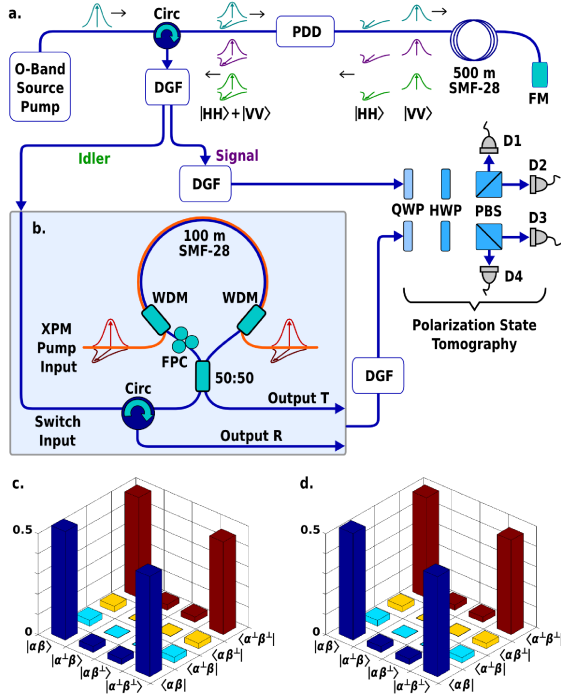


FIG. 1: (a) Entangled photon-pair source and test apparatus for ultrafast switching. Nondegenerate entangled photon pairs ($\lambda_{\text{signal}} = 1303.5$ nm and $\lambda_{\text{idler}} = 1306.5$ nm) are generated in 500 m of standard single-mode fiber (SMF-28). Signal and idler photons are separated using a double-pass grating filter (DGF). Circ: circulator, FM: Faraday mirror, FPC: fiber polarization controller, HWP: half-wave plate, PBS: polarizing beam-splitter, PDD: polarization dependent delay, QWP: quarter-wave plate, WDM: wavelength-division multiplexer. (b) The single-photon switch. The length of the intra-loop SMF-28 is directly proportional to the switching window. An $L = 100$ -m loop (shown) results in a ≈ 200 -ps switching window. (c) Reconstructed density matrix of the unswitched state for $L = 100$ -m (fidelity to a maximally entangled state, $F = 99.5\% \pm 0.2\%$). (d) Density matrix of the switched state for $L = 100$ m ($F = 99.4\% \pm 0.4\%$). Similar reconstructions for the 500-m switch (not shown) yielded $F = 99.5\% \pm 0.2\%$ (unswitched) and $F = 99.2\% \pm 0.2\%$ (switched).

the nonlinear character of the XPM process limits the switching contrast in this type of operation. Because the pump pulse can not be made perfectly square-shaped, the center of the signal pulse receives a stronger nonlinear phase shift than the pulse wings, making it effectively impossible to choose a single pump power which maximizes switching contrast over the entire signal pulse.

Our switch design is immune to each of these two fundamental problems and allows for noiseless, high contrast switching operation. Firstly, the large anti-Stokes detuning (≈ 35 THz) between the 1550-nm pump pulses and the 1310-nm single-photon pulses prevents contamination of the quantum channels by spontaneous Raman scattering from the pump. Secondly, in standard single-mode fiber (the loop medium) this detuning leads to a large group-velocity difference (≈ 2 ps/m) between the

pump and signal pulses. This allows the switch to operate in a regime where the pump pulse walks completely through the signal's temporal mode, providing the type of uniform phase-shift which is essential for high-contrast switching operation. The effective phase shift is therefore determined by the total energy in a single pump pulse, regardless of that pulse's temporal profile. The switching window, τ , is in turn determined—not by the pump power, but—by the *length of the fiber*, L , used in the NOLM. For our case, $\tau = L \times 2$ ps/m. The turn-on time of this switching window is set by the temporal extent of the pump pulses. For 5-nm bandwidth, transform-limited C-band pump pulses, for example, the turn-on time can be as short as 1 ps.

Two key experimental technologies are required to operate and characterize this type of switch: a short-pulse dual-wavelength 1550-nm pump and a source of 1310-nm entangled photons. To create the dual-wavelength pump, two 5-ps duration pulses (1545-nm and 1555-nm wavelengths) are spectrally carved with diffraction gratings from the output of a 50-MHz repetition rate mode-locked fiber laser (IMRA Femtolite Ultra, Model BX-60), which are then multiplexed using a polarization beam combiner (PBC). The power necessary to produce a π phase shift is obtained by amplifying the multiplexed pulses with a cascade of erbium-doped fiber amplifiers (EDFAs). A long-pass filter with a 1543-nm edge is used after each EDFA to ensure that the optical gain is confined to the pump pulses and that no contaminating O-band photons are introduced by the pump preparation process.

The IMRA laser also provides an electrical clock signal for a 1310-nm entangled photon source and an array of four single-photon detectors. The entangled photon source, described in detail in reference [3] and shown in Figure 1(a), utilizes spontaneous four-wave-mixing in standard single-mode fiber to produce pairs of polarization-entangled photons from 100-ps wide, 50-MHz repetition-rate pump pulses at 1305 nm. After switching, the photon pairs are measured with a correlated photon detection system (Nucrypt LLC, Model CPDS-4) consisting of an array of four InGaAs/InP avalanche photodiodes.

In order to test the switch's effectiveness for quantum communications, we measured both active and passive switching of polarization-entangled photon pairs. Figure 1(b) shows the switch as integrated into the fiber-based source of entangled photons referenced above. To test multiple switching windows, loop lengths of 500 m (≈ 900 -ps window) and 100 m (≈ 180 -ps window) were used. The insertion loss introduced by these switches in the O-band quantum channel was measured to be 1.3 dB ($L = 100$ m, port T), 1.7 dB ($L = 100$ m, port R), 1.7 dB ($L = 500$ m, port T), and 2.1 dB ($L = 500$ m, port R). Because all of these directly measured losses include the 0.4 dB or 0.8 dB loss from one or two passes through an optical circulator, the raw switching loss for either transmission

through or reflection from the switching loop is 0.9 dB (1.3 dB) for the $L = 100$ -m (500-m) loop.

To set a performance benchmark for the switch, unswitched (no pump) entangled photons from port R were characterized using coincidence-basis quantum-state tomography [26, 27]. Both signal and idler photons were analyzed using separate quarter waveplate (QWP), half waveplate (HWP), polarizing beam splitter (PBS) combinations, which together perform arbitrary single qubit measurements. The measured coincidence rates—after subtracting accidental coincidences, a procedure which lowers statistical errors—for 36 combinations of analyzer settings [28] were subjected to a numerical maximum likelihood optimization, which reconstructs the density matrix most likely to have produced the measured results. Figures 1(c) and 1(d), respectively, show reconstructed density matrices for passively switched (port R) and actively switched (port T) entangled photons, after reflection or transmission through the $L = 100$ -m loop. Similar reconstructions were performed for the $L = 500$ -m loop; in all four cases, the fidelity of the measured state to a maximally-entangled state exceeded 99.0%. In addition, no measureable state degradation resulted from active versus passive switching.

Another important metric for both quantum and classical routers is the switching *contrast*—or the ratio of power directed to the desired output port divided by the power directed to the complementary output port. Figure 2(a) shows the single-photon switching contrast as a function of the pump-pulse energy. A contrast of 120:1 is achieved at a pump energy of 2.5 nJ for $L = 500$ m. Although the switching contrast is expected to be independent of L , the 100-m data does not appear to achieve full contrast—only 43:1. This artifact is due to a long, low-power tail (≈ 370 -ps total pulse width) in the 1305-nm pump pulses that drive the entangled photon source. Although the entangled photon production rate is proportional to the pump-power *squared*, this still results in a longer than 200-ps pulse width for the entangled photons used to test the switch. As a result, the switching window is too short to completely envelop the photon to be switched, resulting in an artificially lower switching contrast for the $L = 100$ -m loop. We expect the true switching contrast to be the same in both cases ($\geq 120:1$).

Closely related to contrast is the generated single-photon background, from—for example—Raman scattering of the 1550-nm pump pulses. We measured the probability of generating a 1310-nm background photon count and found it to be proportional to L ($\approx 4 \times 10^{-7} \text{m}^{-1}$). This low scattering probability is consistent with the 35-THz Stokes-side detuning of the pump.

In addition to its use as a single-photon router, the switch is a spatio-temporal coupler, enabling the encoding and decoding of quantum information into a temporally multimode Hilbert space, which is, in principle, boundless. The extent to which this Hilbert space can be

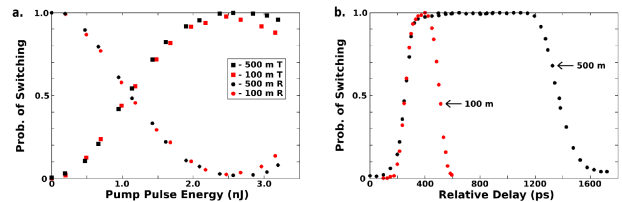


FIG. 2: (a) Single-photon switching contrast. Plot shows the probability of routing an incoming single photon versus pump energy for $L = 500$ m and $L = 100$ m (detector dark counts subtracted). (b) Temporal extent of the switching window, as measured using single photons. Plot shows single-photon counts versus relative delay between the single-photon and the pump pulses (detector dark counts subtracted).

effectively accessed, however, is determined by the temporal switching profiles of the devices described above. To characterize the shape and width of the switching window, we introduce a relative delay between the signal and the pump pulses. Sweeping this delay while measuring the switched single photons we map the switching window (shown in Figure 2(b)). Note that the temporal extent of the photons being switched blurs the true switching window. To quantitatively estimate the extent of this blurring, we directly measure the temporal shape of the 1305-nm pump pulses used to create the test photons. We perform this measurement by constructing a third $L = 2$ -m switch with a switching window of ≈ 10 -ps (full width at half maximum). Using the now-characterized 1305-nm classical pump pulses, we re-measure the switching windows while applying a numerical-fit deconvolution to the results. In this way we obtain the instantaneous temporal widths of the 100-m and 500-m switching windows to be 180 ps and 900 ps, respectively.

The switch's ability to manipulate temporal quantum information has the potential to enable new quantum communication protocols. As an example of this functionality, we use the switch to demultiplex a single quantum channel from a dual-channel entangled photon stream. Consider the hyper-entangled state $|\phi\rangle = c_1|\psi_1\rangle \otimes t_0 + c_2|\psi_2\rangle \otimes (t_0 + \Delta t)$, where $|\psi_1\rangle \equiv \frac{1}{\sqrt{2}}(|HH\rangle + |VV\rangle)$, $|\psi_2\rangle \equiv \frac{1}{\sqrt{2}}(|HH\rangle - |VV\rangle)$, and c_1 and c_2 are arbitrary coefficients. Reconstructing $|\phi\rangle$ using polarization-basis tomography while tracing out any temporal degrees of freedom will yield a highly mixed state, exactly the result one expects from a simultaneous measurement of multiple entangled quantum channels. A temporal switch capable of resolving the two independently entangled channels, however, should be able to measure a single channel's maximal entanglement.

To generate the two temporal channels of entangled photons, we modify our O-band entangled-photon source [3]. Instead of pumping with one pulse, we pump it with a pair of pulses separated by $\Delta t \approx 300$ ps. The delay Δt is obtained using a Michelson interferometer built around a non-polarizing 50:50 beamsplitter. The

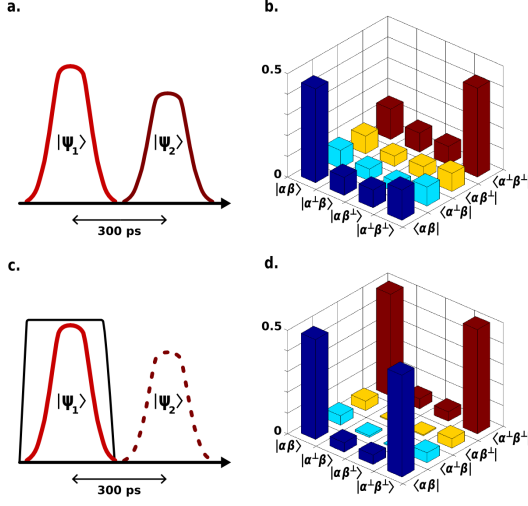


FIG. 3: Demultiplexing a single quantum information channel from a two-channel entangled photon stream $|\phi\rangle = c_1|\psi_1\rangle \otimes t_0 + c_2|\psi_2\rangle \otimes (t_0 + \Delta t)$, where $|\psi_1\rangle \equiv \frac{1}{\sqrt{2}}(|HH\rangle + |VV\rangle)$ and $|\psi_2\rangle \equiv \frac{1}{\sqrt{2}}(|HH\rangle - |VV\rangle)$. (a) Arrangement of detected quantum information channels. (b) Reconstructed density matrix ($F = 58.9\% \pm 0.5\%$). (c) Arrangement of quantum information channels with window for active switching to output T. Because only $|\psi_1\rangle$, and not $|\psi_2\rangle$, is routed to port T for measurement, the resulting demultiplexed state should have high fidelity to a maximally entangled state, even after tracing over the temporal degrees of freedom. (d) Reconstructed density matrix of the demultiplexed state ($F = 98.6\% \pm 0.7\%$).

polarization of the leading and trailing pulses are chosen such that the unnormalized output pump state is $\sqrt{c_1}(|H\rangle + |V\rangle) \otimes t_0 + \sqrt{c_2}(|H\rangle + i|V\rangle) \otimes (t_0 + \Delta t)$. The polarization dependent delay (PDD) in the entangled photon source, t' , now yields four distinct pump pulses $\sqrt{c_1}|H\rangle \otimes t_0$, $\sqrt{c_1}|V\rangle \otimes (t + t')$, $\sqrt{c_2}|H\rangle \otimes (t_0 + \Delta t)$, and $i\sqrt{c_2}|V\rangle \otimes (t + \Delta t + t')$, where $t' = 1.1$ ns [3]. Each pulse drives a spontaneous four-wave mixing process resulting in the signal/idler pairs $c_1|H_s H_i\rangle \otimes t_0$, $c_1|V_s V_i\rangle \otimes (t + t')$, $c_2|H_s H_i\rangle \otimes (t_0 + \Delta t)$, and $-c_2|V_s V_i\rangle \otimes (t + \Delta t + t')$. Notice that the quadratic pump-power dependence has given an $i^2 = -1$ phase on the final pulse. After reversing the PDD in the source, we then generate the desired (unnormalized) state $|\phi\rangle = c_1(|H_s H_i\rangle + |V_s V_i\rangle) \otimes t_0 + c_2(|H_s H_i\rangle - |V_s V_i\rangle) \otimes (t_0 + \Delta t)$. For the demultiplexing test, we choose $c_1/c_2 \approx 1.25$ and $\Delta t \approx 300$ ps.

Figure 3(b) shows the experimentally measured density matrix for the multiplexed quantum channels. As expected, the state is highly mixed; its fidelity to the nearest maximally entangled state is only 58.9%. Utilizing the 100-m switch we then demultiplex (i.e., actively switch) only the first quantum channel ($t = t_0$). As shown in Figure 3(d), after demultiplexing we are able to recover the high fidelity (98.6%) of the target state to a maximally entangled state.

In conclusion, we have demonstrated the first all-

optical single-photon switch suitable for quantum communications. It achieves low-loss (< 1 dB), high-isolation (> 20 dB), and high-speed (< 200 ps) performance without a measureable disturbance to the quantum state of the routed single photons. We demonstrate its ultra-fast capability by demultiplexing a single quantum channel from a time-division-multiplexed stream of entangled photons. Very few fundamental limitations apply to this type of switch design. With carefully designed fiber components, one has the potential to dramatically reduce the switch's loss. Additionally, decreasing L to a few meters will reduce the switch's speed to ≈ 10 ps while simultaneously decreasing the background by an order of magnitude. Even without these improvements, however, this switch represents an important new tool for manipulating temporally-encoded quantum information.

This research was supported in part by the DARPA ZOE program (Grant No. W31P4Q-09-1-0014) and the NSF IGERT Fellowship (Grant No. DGE-0801685).

-
- [1] M. A. Nielsen and I. L. Chuang, *Quantum Computation and Quantum Information* (Cambridge Univ. Pr., 2000).
 - [2] N. I. Nweke, *et al. Appl. Phys. Lett.* **87**, 174103 (2005).
 - [3] M. A. Hall, J. B. Altepeter, and P. Kumar, *Optics Express* **17**, 14558 (2009).
 - [4] M. A. Duguay and J. W. Hansen, *Appl. Phys. Lett.* **15**, 192 (1969).
 - [5] N. J. Doran, and D. Wood, *Opt. Lett.* **13**, 56–58 (1988).
 - [6] K. Hogari and T. Matsumoto, *Appl. Opt.* **30**, 1253–1257 (1991).
 - [7] M. Eiselt, *Electron Lett.* **28**, 1505 (1992).
 - [8] J. P. Sokoloff, P. R. Prucnal, I. Glesk, M. Kane, *IEEE Photon. Technol. Lett.* **5**, 787 (1993).
 - [9] M. Asobe, I. Yokohama, H. Itoh, and T. Kaino, *Opt. Lett.* **22**, 274 (1997).
 - [10] I. Yokohama *et al.*, *J. Opt. Soc. Am. B* **14**, 3368 (1997).
 - [11] G. S. Kanter, P. Kumar, K. R. Parameswaran, and M. M. Fejer, *IEEE Photon. Technol. Lett.* **13**, 341 (2001).
 - [12] J. E. Sharping, M. Fiorentino, P. Kumar, and R. S. Windeler, *IEEE Photon. Technol. Lett.* **14**, 77 (2002).
 - [13] V. Van, *et al. IEEE Photon. Technol. Lett.* **14**, 74 (2002).
 - [14] V. R. Almeida, *et al. Opt. Lett.* **29**, 2867 (2004).
 - [15] G. Bertocchi, *et al. J. Phys. B* **39** 1011 (2006).
 - [16] <http://www.eospace.com>
 - [17] V. R. Almeida *et al.*, *Opt. Lett.* **29**, 2867–2869 (2004).
 - [18] P. Dong, S. F. Preble, and M. Lipson, *Opt. Express* **15**, 9600–9605 (2007).
 - [19] C. Knoernschild, C. Kim, F. P. Lu, and J. Kim, *Opt. Express* **17**, 7233–7244 (2009).
 - [20] K. Uchiyama *et al.*, *J. Lightw. Tech.* **15**, 194–201 (1997).
 - [21] Q. Lin, F. Yaman, and G. P. Agrawal, *Phys. Rev. A* **75**, 023803 (2007).
 - [22] For simplicity, we define “aggregate performance”, in dB units, as: (relative loss) + (relative speed) + (relative production rate of in-band noise photons).
 - [23] H. Bülow and G. Veith, *Elect. Lett.* **29**, 588–589 (1993).
 - [24] K. J. Blow, N. J. Doran, B. K. Nayar, and B. P. Nelson, *Opt. Lett.* **15**, 248–250 (1990).
 - [25] D. Mortimer, *J. Lightw. Tech.* **6**, 1217–12124 (1989).

- [26] D. F. V. James, P. G. Kwiat, W. J. Munro, and A. G. White, *Phys. Rev. A* **64**, 052312 (2001).
- [27] J. B. Altepeter, E. R. Jeffrey, and P. G. Kwiat, *Advances in AMO Physics, Vol. 52*, Ch. 3 (Elsevier, 2006).
- [28] J. B. Altepeter, *et al. Phys. Rev. Lett.* **95**, 033601 (2005).